

## **NONLINEAR SYSTEM IDENTIFICATION OF A NACA 0015 HIGH LIFT SYSTEM UNDER DUAL LOCATION OPEN LOOP CONTROL**

**Bruce Alstrom** <sup>\*(1)</sup>, **Stephane Moreau** <sup>\*(2)</sup>, **Noureddine Atalla** <sup>\*(3)</sup>, **Erik Bollt** <sup>†(4)</sup>, **Pier Marzocca** <sup>‡(5)</sup>

<sup>(\*)</sup> *University of Sherbrooke, 2500 University Boulevard, Sherbrooke, QC, J1K 2R1 Canada*

[Robert.Bruce.Alstrom@usherbrooke.ca](mailto:Robert.Bruce.Alstrom@usherbrooke.ca)

[Stephane.Moreau@usherbrooke.ca](mailto:Stephane.Moreau@usherbrooke.ca)

[Noureddine.Atalla@usherbrooke.ca](mailto:Noureddine.Atalla@usherbrooke.ca)

<sup>(†)</sup> *Clarkson University, 8 Clarkson Avenue, Potsdam New York, USA, 13699*

[ebollt@clarkson.edu](mailto:ebollt@clarkson.edu)

<sup>(‡)</sup> *Royal Melbourne Institute of Technology, PO Box 71 Bundoora VIC 3083, Australia*

*office Bundoora East Campus, Australia*

[pier.marzocca@rmit.edu.au](mailto:pier.marzocca@rmit.edu.au)

### **ABSTRACT**

An NACA 0015 airfoil fitted (with flow control capability) with a simple trailing edge flap set at an angle of attack of 16 degrees (deep stall), flap deflection is set at zero degrees at an airspeed of 5 m/s is the subject of this research. The flow conditions analyzed are an unforced stalled condition and an open loop controlled condition with a modulation frequency of 50 Hz. The analysis is performed using classical signal processing tools along with higher order spectral moments. For the unforced flow condition, the analysis revealed that the autobispectral results are directly related to the RMS pressure distribution especially when there is a vortex shedding frequency present. The analysis also exposed the nonlinear signature of vortex pairing and shredding. For the forced flow condition, it is observed that forcing the flow stabilizes tones that otherwise would migrate downstream of the leading edge. The surface pressure fluctuations are reduced because of convective energy transfers between the forced fundamental of ~43 Hz and low frequency components which results in reattachment of the flow.

### **1. INTRODUCTION**

Periodic excitation has been shown to encourage the regulation of coherent structures in a flow field; this is largely due to the fact that fluid flows are nonlinear and the presence of the nonlinearity creates multiple frequency components. These frequency components can be targeted with the goal of enhancing the strength of the

quadratic phase coupling. Typically, synchronization is detected using frequency spectra. But the spectra can neither provide information about the nonlinear interaction between Fourier modes, nor can they resolve the changes in Fourier components in time. In general, the bicoherence, which is the normalized bispectrum is a measure of the amount of phase coupling that occurs in a signal or between two signals. Phase coupling is said to occur when two component frequencies are simultaneously present in the signal (s) along with their sum (or difference) frequencies and the phase of these component frequencies remains constant. There are two types of bicoherence analysis, the first is Fourier based and the other is wavelet based; the wavelet based option will be used in this research. A formal definition of wavelet bicoherence is provided in Section 3 of this work. Bispectral analysis is applied to a wide variety of nonlinear systems. The focus of this paper is aerodynamic flow systems. The following brief literature review highlight some of these examples in which aerodynamics flows are studied using higher order spectral analysis. Lovato conducted flow control experiments on a NACA 0015 airfoil [1]. It was observed that forcing at the fundamental frequency inhibits vortex pairing, while forcing at the corresponding subharmonic frequencies enhances vortex pairing. Specifically, it was observed that control at the fundamental frequencies prevents shear layer vortex pairing which stops shear layer growth and reduces the separation region. In addition, the overall size of the separation region decreased under tangential-pulsed air open loop forcing

at both fundamental and subharmonic frequencies. Davis et al, [2] followed up with the application of bispectral analysis to the dissertation data collected by Lovato [1]. The purpose of the investigation was to further explain the physical nonlinear mechanisms that govern the frequency modulated control of a separating boundary layer on a static airfoil. The bispectral analysis confirmed that forcing at fundamental frequencies produced energy transfers from the fundamental frequencies to the subharmonics; the reverse is also true when the primary excitation is at the subharmonic frequencies. By forcing the shear layer at a subharmonic frequency, it was found that the open loop control action produced pairing interactions between the shear layer vortices which resulted in the rapid growth of the shear layer. This rapid growth results in the reattachment of the flow. The study also showed that the frequency triads help to identify the optimum forcing frequencies at a specified angle of attack, a feature that may prove useful in the current work. It is important to note that there was no spatial analysis of quadratic phase coupling and the analysis is autobispectral in nature only. Hajj et al conducted experiments in a low turbulence subsonic wind tunnel with a splitter plate in the contraction of the tunnel and a two-component probe downstream. The purpose of the experiment was to quantify the nonlinear and parametric resonance mechanisms that are related to the subharmonic growth in transition to turbulence in-plane mixing layers. Higher order spectral methods were used to investigate the aforementioned mechanisms responsible for the energy transfer to the subharmonic. It was observed that the dominant interaction is a parametric resonance mechanism between the fundamental and the subharmonic modes. This interaction leads to significant growth in the subharmonic. The measurements also show that the fundamental also redistributes energy to the other Fourier modes via a three wave mechanism [3]. For the same experimental set up, Hajj and his colleagues [4] found that when the phase coupling between the fundamental and the subharmonic is high, maximum subharmonic growth is found to occur, which suggested that the phase difference is small. For the same experiment, Hajj et al examined the results to uncover the effect of phase difference and coupling between the fundamental and the subharmonic modes in the transitioning boundary layer. The results show when the phase coupling is high between the fundamental and the subharmonic, maximum growth of the subharmonic mode is enabled. As such the phase difference is close to zero. The results are in fact a graphical representation of the evolution of the phase difference and magnitude of the autobicoherence as a function of position along the chord of the splitter plate. Ritz and his colleagues [5] presented the nonlinear spectral dynamics of a transitioning flow in the wake of a thin flat plate. The measurements were taken at different downstream positions using a two-point

method. The measurement setup consists of two sensors which are separated in the downstream direction. The quadratic transfer function is estimated from the experimental data. The transfer function is not bicoherence, it is the sum of a linear transfer and quadratic transfer functions. The coefficient of the linear term is the linear coherence and the coefficient of the quadratic term is the bicoherence; in this paper, it is referred to as local coherence. Ritz et al defines local coherence as autobicoherence and non-local coherence as the cross-bicoherence; both types of calculation detect phase locking between individual Fourier components. The post processed experimental results show that in the early nonlinear stages of transition, the interactions between modes of similar frequency and frequency component below the fundamental are most effective in redistributing the spectral energy. As the transition evolves, the interaction involving the first harmonic becomes efficient in the spectral energy transfer process. Ritz et al also concluded that the cross-bispectral analysis provides information on the efficiency of frequency coupling, and that the local coherence (autobispectral analysis) characterizes those interactions that result in a power exchange. The effect of the spacing of instrumentation on the nonlinear processes was also discussed. Specifically, when the probes are close together, the linear effects will dominate because the spatial (and temporal) interaction region is very short. The quadratic nonlinear effects in the flow become more important as the measurement devices are space farther apart. Again this observation could prove to be very important to this current research project as a linear sensor array is used. Davila et al. [6] obtained experimental results from two-point measurements of velocity in the planar wake of flat plate. The results showed that there was a clear relationship between spatial linear coherence, the power spectra and the autobicoherence. High spatial linear coherence appears in modes driven by nonlinear interactions. Davila conjectured from the combination of the autobicoherence and spatial linear coherence calculations that the fundamental mode interacts with the instability modes to drive energy into the spectral energy trough seen in the resulting spatial linear coherence plots. In addition, it was observed that the fundamental peak contains nearly all the nonlinear interactions. A good summary of the nonlinear interaction results for the splitter plate experiments obtained by Hajj, Miksad, Powers and other research associates are given in [7]. The current study has two objectives; the first is to identify the nonlinear interactions in the un-forced flow and the interactions that result from the application of open loop control; the second is to understand how the nonlinear interactions contribute to the reduction in the surface pressure fluctuations. The current paper is organized as follows; The experimental set up and hardware is presented in Section 2, followed by the methods of analysis in Section

3. Section 4 discusses the nonlinear characterization of the un-forced flow and Section 5 discusses the nonlinear characterization of a selected forced case for comparison. The summary and conclusions are given in Section 6.

## 2. EXPERIMENTAL SETUP

The experiment is performed on a NACA 0015 airfoil with a simple flap (Figure 1). The wing has a chord of length is 30 cm and has an aspect ratio of 1.33. The NACA 0015 airfoil is equipped with two piezo-based directed synthetic jet actuator arrays (Figure 1, red boxes). Each array has 10 actuators. The wing is fitted with an embedded linear sensor array consisting of 11 pressure transducers. The wing is mounted on a strut that is attached to the sting of an aerodynamic force balance. The experiment is conducted in an open circuit wind tunnel at wind tunnel velocities ranging from 5 m/s to 25 m/s. The wing is configured at an angle of attack 16 degrees and is able to have flap angles ranging from 0 to 40 degrees. The test section was fitted with false walls to facilitate two dimensional flow. The pressure fluctuation data was sampled at 9 kHz for a period of 30s. Three different experiments were conducted; they are Amplitude Modulated Dual Location Open Loop Control, Adaptive Control with Amplitude Modulation using Direct Sensor Feedback and Adaptive Control with Amplitude Modulation using Extremum Seeking Control. Only the open loop control results will be presented here.

The data is collected using the DS1103 PPC Controller Board which is specially designed for the development of high-speed multivariable digital controllers and real time simulation. It is a real time control system based on a Power PC processor. The dSPACE 1103 ACE Kit provides a means by which researchers can rapidly develop controller and implement control system designs and assess their performance. dSPACE has been used extensively in closed loop active flow control. The DS1103 board has a bus frequency of 133 MHz. It also has 16 mixed channels equipped with 4 sample and hold analogue to digital conversion (ADC) with 16-bit resolution and 4 channels each equipped with one sample and hold ADC. The schematic below shows (Figure 2) the integrated system used in the experiment. The following section will discuss how the data collected by this system is analysed.

## 3. DATA ANALYSIS THEORY AND METHOD

The pressure signals are generally noisy. In order to remove the noise from the signal in a holistic manner, the signal was truncated and then averaged; it was found that other methods of filtering might introduce spectral artifacts when performing signal processing. For these

experiments, all the data records are 30 s in length and sampled at 9 kHz. When the data record (with time) is time averaged, the resulting number of samples is 40,000. The frequency resolution at 9 kHz is 0.225 Hz for 40,000 samples. The analysis performed in this work is accomplished using a combination of classical linear signal processing methods (specifically FFTs and wavelet based linear spatial coherence analysis) and wavelet based higher order spectral analysis, specifically, the autobispectral analysis (for sensor positions along the wing chord), cross-bispectral analysis (for tracking of convected quadratic phase coupling) and time-frequency analysis if required. Time-frequency analysis is concerned with identifying and quantifying oscillatory components present in real-life signals. This achieved by projecting the signal onto the time-frequency plane, which enables one to study the properties of the signal in time and frequency at the same time. These projections are called time-frequency representations (TFRs). The analysis in this paper utilizes the wavelet transform. The continuous wavelet transform has logarithmic frequency resolution. The wavelet transform of a function  $s(t)$  is defined as:

$$W(\xi, \tau) = \int_{-\infty}^{+\infty} s(t)\psi_{\xi, \tau}^*(t)dt \quad [1]$$

Where  $\xi$  and  $\tau$  are scale and time variables respectively;  $\psi_{\xi, \tau}^*(t)$  represents the wavelet family generated by continuous translations and dilations of the mother wavelet. The translations and dilations are obtained by:

$$\psi_{\xi, \tau} = \frac{1}{\sqrt{\xi}}\psi\left(\frac{t-\tau}{\xi}\right) \quad [2]$$

The wavelet to be used for this analysis is the log-normal wavelet. It is defined as follows:

$$\psi(t) = e^{-\frac{2\pi f_o \log t}{2}} \quad [3]$$

In this definition,  $f_o$  is chosen to be 3. This wavelet transform is the basis for the time-frequency linear coherence and bispectral analysis. The wavelet cross power spectrum is defined as:

$$P_{xy}^w(\xi) = \int_T W_x^*(\xi, \tau)W_y(\xi, \tau)d\tau \quad [4]$$

The cross coherence calculation is used to examine the coupling between the 11 pressure sensor locations in series caused by the vortical structures that are convected downstream of the leading edge. The normalized wavelet cross-spectrum (wavelet linear coherence) is defined as:

$$C_{xy}^w(\xi) = \frac{|P_{xy}^w(\xi)|^2}{P_{xx}^w(\xi)P_{yy}^w(\xi)} \quad [5]$$

$C_{xy}^w(\xi)$  is bounded by 0 and 1. A coherence magnitude of 0 means that there is little to no coupling and a value of 1 means that there is perfect coupling; values in between the two bounds are indications of partial coupling. Wavelet bicoherence is a measure of quadratic phase-coupling in a single signal or between two signals (cross-bicoherence). Quadratic Phase Coupling (QPC) is said to have occurred when two frequencies  $f_1$  and  $f_2$ , are present in the signal at the same time along with the sum (or difference) of the two frequencies and the sum of phases of these frequencies remains constant. The magnitude of the bicoherence ranges between zero and unity; complete quadratic phase-coupling happens when the bicoherence is one or closed to one. The two Fourier components are decoupled when the bicoherence magnitude is close to zero or equal to zero. If the nonlinearity is greater than order 2, then it is also possible to obtain zero magnitude for the bicoherence and higher-order spectra has to be investigated to unveil higher-order phase-coupling. The second wavelet based spectral moment to be used in this analysis is an autobicoherence and is defined as follows:

$$\frac{|b_{xxx}^w(\xi_1, \xi_2)|^2}{|B_{xxx}^w(\xi_1, \xi_2)|^2} = \frac{(\int_{\tau} |W_x(\xi_1, \tau) W_x(\xi_2, \tau)|^2 d\tau)}{(\int_{\tau} |W_x(\xi, \tau)|^2 d\tau)} \quad [6]$$

The third wavelet based spectral moment to be used in this analysis is a cross-bicoherence and is defined as follows:

$$\frac{|b_{yxx}^w(\xi_1, \xi_2)|^2}{|B_{yxx}^w(\xi_1, \xi_2)|^2} = \frac{(\int_{\tau} |W_x(\xi_1, \tau) W_x(\xi_2, \tau)|^2 d\tau)}{(\int_{\tau} |W_y(\xi, \tau)|^2 d\tau)} \quad [7]$$

The analysis in this paper utilizes the wavelet transform only. The analysis sequence for this research is executed in the following manner; the analysis begins with calculating the FFTs for each sensor location or station followed by an autobicoherence calculation. The autobicoherence analysis is used to examine the nonlinear interactions between frequency components at each sensor station/location. In addition, the analysis allows observing the relationship between the magnitude of the bicoherence and the RMS pressure fluctuation distribution. In order to understand how the nonlinear interactions, move along the chord, two configurations of analysis for the linear sensor array will be used. They are illustrated in the figure below (Figure 3). The arrows point in the direction of the aerodynamic flow.

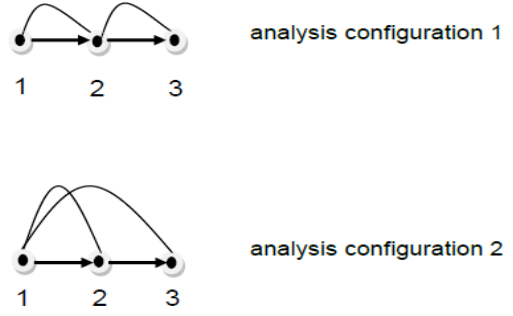


Figure 3.0 Schematic linear array analysis configurations

The first type involves examining the linear spatial coherence in a point-to-point manner. This is repeated for the cross-bicoherence analysis. The configuration allows studying the smaller structures in the flow. The assumption must be made that the frequency components are both linear and nonlinear. The second configuration involves selecting a reference location. The same will be done for the cross-bicoherence. The direction of analysis is from the leading edge to the trailing; the results are aerodynamic in nature. If the direction is reversed, the results are acoustic.

The second analysis configuration provides information about the larger structures in the flow. In the bicoherence analysis, features on the diagonal and the off diagonal regions of the contour map are examined. In order to quantitatively describe the features seen in the map, a new parameter must be defined. The bicoherence map is presented in a Cartesian manner and as such we can take advantage of this feature; the contour growths along lines of constant frequency can be described by the length of a line (See red arrow in Figure 4).

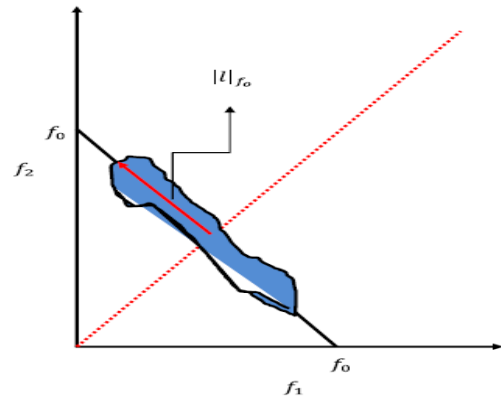


Figure 4.0 Schematic of contour map

The arrow is placed at the center of mass on major axis of the contour along the line of constant frequency,  $f_0$ . This parameter can be used on any of the diagonals in the

bicoherence matrix. The length parameter  $|l|_{f_0}$  is given as follows:

$$|l|_{f_0} = \left[ [f_{1,2} - f_{1,1}]^2 + [f_{2,2} - f_{2,1}]^2 \right]^{0.5} \quad [8]$$

The next section presents the results derived from the theory and analysis configurations described above.

#### 4. RESULTS AND DISCUSSION: ANALYSIS OF THE UN-FORCED FLOW

The analysis begins with examining the frequency spectra (Figure 5) of the un-forced separated flow ( $U= 5$  m/s,  $\alpha = 16^\circ$ ,  $\delta_f = 0^\circ$ ). The results of the FFT survey was conducted and the frequencies are tabulated in Table 1. Table 1 shows the frequency components at each chordwise station. The reader will see that there are tones that persist from leading edge to trailing edge. Namely,  $\sim 33.5$  Hz and its superharmonic at  $\sim 66$  Hz. At sensor stations downstream of the leading edge, it is observed that other frequencies begin to appear. For example, at  $x/c=0.3760$ , a 14.28 Hz tone begins to show. Figure 6 shows the variation of the surface pressure fluctuations as a function of sensor position. The pressure fluctuations increase toward the trailing edge (about main spectral peak at  $\sim 33.5$  Hz) indicates that the flow is separated from the wing. From this point on, the sensor locations will be referred to as 'Station' for the sake brevity i.e.  $x/c=0.1826$  is Station 1 and so on.

Chordwise Location (X/C)	Frequencies (Hz)
(Station 1) 0.1826	33.5, 65.37, 132.5, 144.7, 166, 236.8, 270, 359.5
(Station 2) 0.2293	33.5, 132.5, 236.8, 359.5
(Station 3) 0.266	33.5, 59.6, 132.5, 236.8, 359.5
(Station 4) 0.3026	33.5, 65.37, 132.5, 166, 236.8, 359.5
(Station 5) 0.3393	33.5, 65.37, 132.5, 166, 236.8, 270, 359.5
(Station 6) 0.376	14.28, 33.5, 65.37, 92, 111, 132.5, 166, 236.8, 359.5
(Station 7) 0.4126	14.28, 33.5, 65.37, 132.5, 166, 236.8, 270, 359.5
(Station 8) 0.4493	14.28, 33.5, 65.37, 111, 132.5, 144.7, 166, 187.3, 236.8, 270, 359.5
(Station 9) 0.7483	14.28, 33.5, 65.37, 132.5, 166, 236.8, 270, 326, 359.5, 393
(Station 10) 0.7846	14.28, 33.5, 65.37, 111, 126, 132.5, 144.7, 166, 236.8, 270, 326, 359.5, 393
(Station 11) 0.821	14.28, 33.5, 65.37, 132.5, 144.7, 166, 236.8, 270, 326, 359.5, 393

Table 1. Main tone frequencies in FFT Survey for Un-Forced Separated Flow

The autobicoherence maps (Figure 7) show that at sensor locations 1, 3,5,6,7,9 and 11 there is quadratic phase coupling at ( $\sim 17$  Hz,  $\sim 17$  Hz,  $\sim 33.5$ - 34 Hz). Note that there is some variability in the frequency tagging due to cursor placement. The  $\sim 33.5$ - 34 Hz is the fundamental seen in the FFTs (See Figure 5). At Stations 2, 8 and 10, the dominant autobicoherence contour growths on the 30 Hz line of constant frequency are separated into two lobes; or put another way, the contours do not extend to touch the principle diagonal of the bicoherence matrix. The geometric length of the contour growths along the 30 Hz line generally increases with the magnitude of the surface pressure fluctuations. The spreading of the contours means that the resulting frequency triple ( $\sim 34$  Hz) is exchanging energy with over a bandwidth ranging from 3 Hz to 30 Hz approximately. This result agrees well with the published results on quadratic phase coupling in fluid systems. This explains the clustering of bicoherence contours over the geometric region  $[0 < f_1 < 25 \text{ Hz}, 0 < f_2 < 25 \text{ Hz}]$ . Table 2 shows how the geometric contour length  $|l|_{30 \text{ Hz}}$  varies as a function of chordwise position; this parameter also varies with the magnitude of the main spectral peak (33-34 Hz) observed in FFTs

Chordwise Location (X/C)	Pressure (kPa) at $\sim 33$ -34 Hz	$ l _{30 \text{ Hz}}$
(Station 1) 0.1826	1.481	6.3704
(Station 2) 0.2293	1.491	5.3058
(Station 3) 0.266	0.7761	8
(Station 4) 0.3026	1.331	5.3542
(Station 5) 0.3393	2.415	13.1722
(Station 6) 0.376	2.334	14.6
(Station 7) 0.4126	3.361	8.422
(Station 8) 0.4493	3.328	4.5845
(Station 9) 0.7483	6.582	16.5
(Station 10) 0.7846	5.939	10.67
(Station 11) 0.821	6.447	15

Table 2. Variation of  $b^2(f_1, f_2)$  Contour Length with Position & Pressure

The average magnitude is  $\sim 9.8$  Hz, with the highest magnitude at 16.5 Hz (roughly half of the fundamental frequency) at Station 9 and the lowest at 4.58 Hz at Station 8. In the top left corner of each map, between 30-40 Hz, the reader will observe a contour evolves along the chord of the wing. At Station 1, note that there is no quadratic phase coupling between 30- 40 Hz. At Station 2, we observe a contour growth which continues to evolve until Station 8. At Station 8, the phase coupling weakens considerably; it is possible that Station 8 is

located at the boundary between two coherent structures on the surface of the airfoil. This may explain the increased RMS pressure (Figure 6) and the weak quadratic phase coupling at Station 8. The contour is geometrically centered on ( $\sim 11$  Hz, 34 Hz,  $\sim 45$  Hz). It can be concluded that this frequency triple is nonlinear in nature. The nonlinear tone is thought to be the result of vortices merging at Station 2 and terminating at Station 8 and re-emerges on the trailing edge flap. The remaining three stations show that the nonlinear tone is spreading has a bicoherence magnitude greater than  $\sim 0.2$ . From Station 3 onward, a similar feature is observed for a  $\sim 53$  Hz nonlinear tone. The  $\sim 53$  Hz tone undergoes contour spreading at Stations 7 and 11. The second harmonic at  $\sim 66$  Hz does not appear in the autobispectral results; this suggests that the harmonic may be a nonlinear tone as well. The autobicoherence results also provide a good indication of what frequencies the flow is most receptive to being forced at for a given airspeed and angle of attack. In this instance they are 10 Hz, 20 Hz, 30 Hz, 34 Hz,  $\sim 43$  Hz and  $\sim 53$  Hz. The following general features were observed in the autobicoherence maps:

- Highly organised contours along lines of constant frequency;
- Elongation and spreading of contours. The contour elongation correlates with changes in the magnitude of the main spectral peak at  $\sim 33$ -34 Hz. The spreading of the contours can be attributed to the generation of other spectral peaks.

Similar features were observed by Elgar and his colleagues [8]; for a vibrating cylinder subjected to a low Reynolds number cross flow revealed that quadratic phase coupling contours grew along lines of constant frequency. These lines corresponded to the spectral peaks found in the power spectra. The contours generally stretched when magnitude of the spectral peaks increased and contracted when the peaks decreased in magnitude. Closely spaced tones (or side bands- tones that split off from a main spectral peak). Elgar et al. also discuss the presence of evolving shedding regimes; this occurs when the wake velocity fields change over a very short period of time. The changing wake velocity field resulted in spectral peaks that emerge and then disappear. Similar behavior was observed in this experiment.; the  $\sim 43$  Hz,  $\sim 53$  Hz and 66 Hz tones evolved over the chord length of the airfoil. Recent work on nonlinear systems subjected to closed loop persistent excitation revealed that it was a necessary condition to have a main spectral peak for frequency entrainment to exist along with quadratic phase coupling. These two mechanisms together formed for synchronisation. A separated wake resulting from a symmetric airfoil in deep stall is essentially a self-synchronised system. This part of the analysis will be used as a reference for the spatial linear coherence and

cross- bispectral analysis that follows. The next part of this analysis uses *analysis configuration 2*.

Figure 8 shows the evolution of the spatial coherence along the chord of the airfoil. Across the sensor pairs there are several frequencies that appear regularly, they are  $\sim 33.5$ -34 Hz,  $\sim 132$  Hz, 166 Hz and  $\sim 230$  Hz. At frequencies less than 50 Hz, it is observed that there are closely spaced tones with a linear coherence over  $\sim 0.3$ . This corresponds to the then densely packed phase coupling contours in the lower left corner region of the autobicoherence maps. Of these closed space tones,  $\sim 14$  Hz and  $\sim 20$  Hz are distinct and have a high linear coherence. This frequency pair also form the fundamental at  $\sim 33.5$ -34 Hz this is also highly correlated linearly. Beginning at sensor pair (1,4), the superharmonic at  $\sim 66$  Hz, shows an increase its coherence magnitude indicating that a flow structure with this frequency is convecting downstream of the leading edge. This observation is made because of the weak linear coupling of  $\sim 66$  Hz at the sensor pairs before (1,4). For sensor pairs (1,5) and (1,9), it can be observed that there is a marked increase in coherence magnitude over band from 50 Hz on (the window size was selected to magnify the lower frequencies). In between these locations and after Station 9 (located on the trailing edge flap), the coherence drops below 0.2 except at frequencies identified earlier. The coherence magnitude for the superharmonic (at  $\sim 66$  Hz) at (1,5) is 0.54 and 0.66 at (1,9). It is conjectured that there are two cells on the surface of the wing and Stations 5 and 9 are the locations of the leading edges of the cells. For the cross-bicoherence analysis, we will focus the readers eyes on the following lines of constant frequency, they are the 30 Hz line, the 40 Hz line. Like the autobicoherence results the contour growths along the 30 Hz line show high coupling strength as expected. Note that the cross-bicoherence contours for the fundamental present as lobes in the 30 Hz line and do not stretch like their autobicoherence counterparts.

It was pointed out in the examination of the bicoherence results that there are three tones that are transient in the sense that they emerge and terminate at different location along the chord of the wing. They are  $\sim 43$  Hz,  $\sim 53$  Hz and  $\sim 66$  Hz. For the  $\sim 43$  Hz tone, it is observed that all sensor pairs except (1,4) there is a contour growth that straddles the matrix diagonal line. For the  $\sim 66$  Hz tone, at sensor pair (1,4), note the bright yellow band; this correlates to the emerging linear coherence peak observed in Figure 5 (sensor pair 1,4). The center of mass of the contour is located at approximately ( $\sim 33$  Hz,  $\sim 33$  Hz,  $\sim 66$  Hz) for sensor pairs (1,5), (1,7), (1,9) and (1,11). In Figure 5, it was observed that the sensor pairs (1,5) and (1,9) identified a large increase in linear spatial coherence beginning at 50 Hz. The  $\sim 66$  Hz tone showed a high levels of linear coupling.; the cross-bicoherence at these same locations show that the contours spread

significantly. The largest area for the ~ 66 Hz tone can be observed for sensor pair (1,9). At the location where the contour spreading occurs, visually it appears that the densely packed contour region (at  $f < 50$  Hz), the quadratic phase coupling weakens at some of the smaller frequencies. Note that the quadratic phase coupling at ~66 Hz is less than 0.1, however it the growth of the contour that we are interested in; the spreading at ~66 Hz corresponds to the linear coherence identified in Figure 8 at sensor pairs (1,5) and (1,9).

## 5. RESULTS AND DISCUSSION: ANALYSIS OF THE FLOW UNDER OPEN LOOP CONTROL

The open loop control task was conducted using dual location excitation similar to that described by Greenblatt [9]. For our experiment, the feedforward control signal used was an amplitude modulated sinewave given by:

$$V(t) = A_{\text{amp}} (\sin \omega_m t) \sin(\omega_{c(\text{LE,TE})} t + \phi_c) \quad [9]$$

Note that the directed synthetic jet arrays are operated at different carrier frequencies, specifically the leading array operated at 1195 Hz and the trailing edge array at 1197 Hz. The phase angle is used alternate the momentum addition cycles of the synthetic jet arrays with respect to each other. The modulation frequency, which is typically aimed at exciting the frequency based region of receptivity. For this experiment, the modulation/forcing frequency was varied from 5 Hz to 100 Hz and the phase angle was fixed at zero. Figure 10 shows the RMS pressure distribution that result from the open loop forcing at discrete frequencies for the clean wing configuration ( $\alpha = 16^\circ$ ,  $\delta_f = 0^\circ$ ). The forced RMS pressure distribution shows a marked sensitivity to the changes in modulation/forcing frequency. Superimposed on this plot is the un-actuated RMS pressure distribution for comparison. In each case, the synthetic jet actuators create a pressure fluctuation ‘hump’ on the upper to leading edge portion of the chord which agrees well with the experimental results presented in [10] and [11]. Note that there are three groupings of frequencies; Group 1 (70 Hz and 90 Hz), Group 2 (5 Hz, 10 Hz, 20 Hz, 25 Hz, 30 Hz, 35Hz, 45 Hz and 80 Hz) and Group 3 (40 Hz, 50 Hz and 60 Hz). These groupings of frequencies characterise the receptivity of the flow. Groups 2 and 3 show a reduction in the surface pressure fluctuation hump and the leading edge of the airfoil as compared to Group 1. Group 2 shows that the flow is frequency locked over a large range of frequencies as compared to Groups 1 and 3. In general, the surface pressure fluctuations show a marked reduction after  $x/c = 0.4126$  (Station 7). It is also important to note that Group 2 corresponds to the dense region of contours identified by the un-forced autobicoherence, cross-bicoherence and spatial linear

coherence analyses. For comparison, the open loop control case with a modulation frequency of 50 Hz (from Group 3) is selected for analysis. An FFT survey reveals that there are several frequencies of interest; they are 6.45 Hz (subharmonic), 10.85 Hz, 43.40 Hz (fundamental), 83.22 Hz (superharmonic), 200 Hz, 240 Hz and ~360Hz. From Stations 1 through 4, it is observed that there are broadband pressure fluctuations from about ~30 Hz onward. After Station 4, the fluctuation amplitude decreases significantly. Based on Figure 10, the first seven pressure transducers represent the *lock in* distance for the flow; The reduction in pressure fluctuations according to the frequency spectra takes place within the first seven transducers. According to Figure 10, for 50 Hz, the surface pressure fluctuations are significantly lower than the un-forced flow, indicating that the flow is attached; this correlates with the reduction in the pressure fluctuation amplitude seen in the spectra (Figure 11). Note that 43.40 Hz is forced vortex shedding frequency.

For the linear coherence analysis (Figure 12), it is observed that ~43 Hz tone is the new stabilized shedding frequency. The term stabilised in this context means that the tone is not evolving with distance, it is a standing frequency. The average linear coherence across the sensor pairs is ~0.64. Note that in the un-forced case, the spatial transient tones were not constant over the chord length; thus forcing the flow may indeed have stabilized this type of nonlinear frequencies. Nonlinear systems that are capable of exhibiting chaotic behaviour have embedded inside the its attractor, many admissible orbits that are unstable; by forcing the system at a given frequency, it is possible to stabilize the system about one of the admissible periodic orbits. For sensor pairs (1,2), (1,3) and (1,4) show a 67-70 Hz tone with coherence magnitude greater than 0.2. These three sensor stations are located in the region where the pressure fluctuation hump is located. Beyond Station 4, the 67-70 Hz tone appears to be suppressed. It was observed for the un-forced case that sensor pairs (1,5) and (1,9) showed a marked increase in spatial coherence starting at 50 Hz. For the same sensor pairs under forced conditions, it is observed that the modulation frequency of 50 Hz appears to have un-coupled (linearly) the frequencies resulting in the lack of coherence. This result suggests that the coherent structures observed in the un-forced flow are no longer present.

The open loop control autobicoherence maps (Figure 13) reveal that for the first three stations, there are broken contours about the 40 Hz line of constant frequency; in fact, the first two sensor stations show what appear to be contours that form an arc to which the 40 Hz line is a tangent (see white line at map 1, Figure 13). Unlike the un-controlled flow, there are no appreciable contour growths along the 40 Hz line of constant frequency. At Station 3 there are lobes, at Station 4 there are no

contours. At Station 5, there is a contour growth along the 40 Hz line but centered on the diagonal of the matrix. Similar observations can be made for the other sensor station about the contours on the 40 Hz line. This result suggests that when the flow is forced at a discrete frequency, it provides decoupling along the region about the 40 Hz line. At Stations 5, 7, 8 and 9, indicated by black arrows, show the contour that is centered on (~40 Hz, ~43, 83 Hz) is in fact the superharmonic of the forced fundamental of 43 Hz. The quadratic phase coupling is around ~0.1 but at each of these locations, the contour spreads. At Stations 7 and 8, this contour spreads along its respective line of constant frequency and toward the origin along the diagonal of the bicoherence matrix. All of the sensor stations show dense contours at frequencies less than 30 Hz. Specifically, at Station 4, the contours in this region appear to be sparse and the same is true for Stations 3 and 10; these locations do not have any quadratic phase coupling at frequencies greater than say 50 Hz. As such there is no local energy exchange with the fundamental or higher harmonics, thus the phase coupling appears to be weakened. The remaining stations show quadratic phase coupling at frequencies greater than 50 Hz and hence the contours at frequencies less than 50 Hz are organized and closely spaced. The concentrated energy exchange at the lower frequencies are responsible for the reduction surface pressure fluctuations because there is a subharmonic at 6.45 Hz which facilitates frequency entrainment along with quadratic phase coupling; this provides the suppression seen in the RMS pressure distributions and the given frequency spectra (Figures 10 and 11 respectively). It was pointed out earlier that the autobicoherence results (See Figure 13) do not show any significant contour growths along the 40 and 80 Hz lines; but in the cross-bicoherence results (Figure 14), it is observed that there are substantial contour growths along the 40 Hz line compared to the those in seen in Figure 13. There are some sparse contour growths along the 80 Hz line (not shown here); this result indicates that the 43 Hz tone observed in the frequency and coherence spectra, convects downstream, thus the energy transfer between the forced fundamental and the lower frequencies is convected downstream also.

## 6. CONCLUSIONS

In this study the surface pressure fluctuations of a symmetric airfoil in deep stall are examined using higher order spectral analysis which are related back to the classical spectral moments. For the un-forced flow, it was observed that the autobicoherence directly relates to the RMS pressure distribution. For example, as the RMS pressure magnitude of the fundamental shedding frequency increases, the bicoherence contours stretch along the corresponding line of constant frequency; the strength of the quadratic phase coupling also increases.

The fundamental frequency also transfers energy to the lower frequencies as seen in the auto and cross-bicoherence results. The auto and cross-bicoherence results also reveal the presence of spatially transient tones that correspond to vortex pairing and shredding. Using the linear spatial coherence, it was observed that there was a broadband increase in the coherence magnitude starting at 50 Hz for sensor pairs (1,5) and (1,9); these are the leading edges of two coherent structures embedded in the separated flow. A separated flow is highly synchronized and phase coherent; for this to happen both frequency entrainment and quadratic phase coupling must be present. For the open loop control case, it was found that the spatially transient tones are stabilized by a discrete input frequency; in this instance that tone is 43.40 Hz. Although the forced shedding frequency is stabilized, it does not appear significantly in the autobicoherence maps but it appears in the cross-bicoherence maps. As such it is conjectured that the local energy transfer that typically takes place between the fundamental and other frequencies is convective in nature. It is this convective energy transfer that is responsible for the reduction in surface pressure fluctuations seen in the RMS pressure distribution curves and the frequency spectra. Lastly, the formation of the two coherent structures identified (using the linear spatial coherence) are suppressed by forcing the flow with modulation frequency at 50 Hz (which is close to ~53 Hz). Further study is required to confirm that the forced shedding frequency consistently does not appear in the autobicoherence analysis.

## ACKNOWLEDGEMENTS

This experimental work was originally supported by the U.S. Airforce Office of Scientific Research (AFOSR) and Clarkson University. The current work is supported by a MITACS Accelerate Post Doctoral Fellowship at the University of Sherbrooke. The authors would like to thank AFOSR and greatly appreciate the support from the University of Sherbrooke Aeroacoustics Group.

## REFERENCES

- [1] Lovato, Julie Anne, 'Active Control of the Separation Region on a Two-Dimensional Airfoil', Ph.D Thesis, Department of Mechanical & Materials Engineering, Washington State University, May 1992.
- [2] Davis, W., Lovato, J., Pezeshki, C., 'Nonlinear Spectral Characterization of Frequency-Modulated Control Applied to a Static Airfoil Shear Layer', 25th AIAA Fluid Dynamics

Conference, June 20-23, Colorado Springs CO.,  
1994, AIAA-94-2217

- [3] Hajj, M.R., Miksad, R.W., Powers, E.J., 'Subharmonic growth by parametric resonance', *Journal of Fluid Mechanics* Vol. 236 (1992), pp 385-413
- [4] Hajj, M.R., Miksad, R.W., Powers, E.J., 'Fundamental-subharmonic interaction: effect of phase relation', *Journal of Fluid Mechanics* Vol. 256 (1993), pp 403-426
- [5] Ch., P., Ritz, E.J., Powers, Miksad, R.W., Solis, R.S., 'Nonlinear spectral dynamics of a transitioning flow', *Physics of Fluids* 31 (12), 1988.
- [6] Davila, J., Hajj, M.R., Miksad, R.W., Powers, E.J., 'Spatial coherence in the wake of a flat plate', *ASME Applied Mechanics Review* Vol. 50 No. 11, Part 2, November 1997.
- [7] Hajj, M.R., Miksad, R.W., Powers, E.J., 'Perspective: Measurement and Analyses of Nonlinear Wave Interactions with Higher-Order Spectral Moments', *ASME Journal of Fluids Engineering* Vol. 119, March 1997.
- [8] Elgar, Steve, Van Atta, C.W., Gharib, M., 'Cross-Bispectral Analysis of a Vibrating Cylinder and Its Wake in Low Reynolds Number Flow', *Journal of Fluid and Structures* Vol.4, pp59-71,1990
- [9] Greenblatt, David, 'Dual Location Separation Control on a Semi-Span Wing', 23rd AIAA Applied Aerodynamics Conference, June 6-9, 2005, Toronto, Ontario Canada, AIAA-2005-5085
- [10] Chang, R.C., Hsiao, F.B., Shyu, J.N., 'Forcing Level Effects of Internal Acoustic Excitation on the Improvement of Airfoil Lift Performance', *Journal of Aircraft*, Vol. 29, No. 5, Sept-Oct 1992.
- [11] Hsiao, F.B., Shyu, J.N., Liu, C., 'Control of Wall-Separated Flow by Internal Acoustic Excitation', *AIAA Journal*, Vol. 28, No. 8, 1990.